

Nonlocal modulations on the temporal and spectral profiles of an entangled photon pair

Silvia Viciani, Alessandro Zavatta, and Marco Bellini*

Istituto Nazionale di Ottica Applicata, Largo E. Fermi, 6, I-50125 Florence, Italy

(Received 17 November 2003; published 3 May 2004)

We present an experimental and theoretical analysis of the energy-time entanglement properties of a two-photon state generated by pulsed spontaneous parametric down-conversion. Different methods of spectral or temporal shaping of one of the two photons have allowed the observation of nonlocal modulations in the autocorrelation or in the spectrum of the other, by coincidence measurements. Either a monochromator or etalon filters have been used to shape the idler photon while observing the conditioned signal autocorrelation with a Michelson interferometer. Alternatively, the unbalanced interferometer has been used to shape the signal photon while measuring the conditioned idler spectrum with the monochromator. The role of the pump spectrum has been investigated by shaping it with additional filters. A theoretical treatment has allowed us to completely describe all the observed features as a function of the different experimental parameters.

DOI: 10.1103/PhysRevA.69.053801

PACS number(s): 42.50.Dv, 03.65.Ud

I. INTRODUCTION

One of the most surprising consequences of quantum mechanics is the entanglement of two or more distant particles. Entanglement is connected with the concept of nonlocality or action at a distance, according to which the measurement of an observable on one particle of an entangled pair determines with certainty the outcome of a conditional measurements performed on the same observable of the other particle, even if the pair is well spatially separated. Nonlocal effects have been objects of discussion since 1935, when Einstein, Podolsky, and Rosen [1] formulated the principle of locality, suggesting the apparent incompleteness of the quantum-mechanical description of nature. In 1964 Bell [2] formulated an inequality which can be used to distinguish between local theories and quantum mechanics: a violation of Bell's inequalities can be considered an evidence of nonlocal effects. Since then, several experiments have been performed to test Bell's inequalities, using different sources of entangled particles, and they have all shown the nonlocal features of quantum effects.

Spontaneous parametric down-conversion (SPDC) of laser light in nonlinear crystals is the currently most practical and efficient source of entangled particle pairs for the test of Bell's inequalities and nonlocality. In SPDC, the annihilation of a pump laser photon of frequency ω_p and momentum \mathbf{k}_p inside the crystal gives simultaneous birth to a pair of quantum correlated photons, named signal and idler, with frequencies ω_s and ω_i and momenta \mathbf{k}_s and \mathbf{k}_i , which must obey energy and momentum conservation ($\omega_p = \omega_s + \omega_i$, $\mathbf{k}_p = \mathbf{k}_s + \mathbf{k}_i$) [3]. Experimental observation of nonlocal effects has been obtained in different ways: by the violation of Bell's-type inequalities in experiments on photon polarization correlations [4–7]; by the observation of fourth-order interference effects among distant interferometers in experiments of

the kind first suggested by Franson [8] on photon time-position correlations [9–13]; and by the observation of “ghost” interference or diffraction effects in experiments on photon momentum correlations [14–17]. Experiments in which nonlocal effects are studied in the time domain suggest the possibility to analyze the same effects in the energy or frequency domain [18–20].

In a recent work [21] we experimentally analyzed nonlocal effects in the frequency-time domain for photon pairs generated in a pulsed parametric down-converter. We showed that by either spectrally or temporally shaping one beam of the pair the other one is, respectively, temporally or spectrally shaped, when observations are made in coincidence. The spectral shaping was obtained by using a monochromator on the idler path, while the temporal shaping by using a Michelson interferometer on the signal path. In particular, we demonstrated that by narrowing the spectrum of the idler photons fourth-order temporal interference fringes appear on the conditioned signal autocorrelation function also for delays much longer than the signal coherence time; alternatively, we pointed out that when the interferometer on the signal path is unbalanced fourth-order ghost spectral interference fringes appear in the conditioned idler spectrum.

Here we present an experimental and theoretical analysis of the same nonlocal effects, using two different kinds of nonlinear crystal (type-I and type-II BBO crystals) and different methods of spectral filtering in order to fully explore the rich possibilities involved in the process. In particular, we use a monochromator with adjustable central frequency and width, and air-spaced etalons with different free spectral ranges (FSRs) and peak widths (full width at half maximum, FWHM). We show that different temporal shaping of the signal autocorrelation function, conditioned on the detection of the filtered idler photon, is observable when different spectral filters are used. When the idler photon is filtered by etalons, the periodic spectral transmission function of the filters induces a modulation in the signal temporal shape, so that the signal autocorrelation function, measured in coincidence, shows temporal modulations with a period equal to the inverse of the FSR. Note that, our experiments relying on a pulsed laser source, the spectral shape of the pump pulses

*Also at European Laboratory for Nonlinear Spectroscopy (LENs) and Istituto Nazionale per la Fisica della Materia (INFM), Florence, Italy. Electronic address: bellini@inoa.it

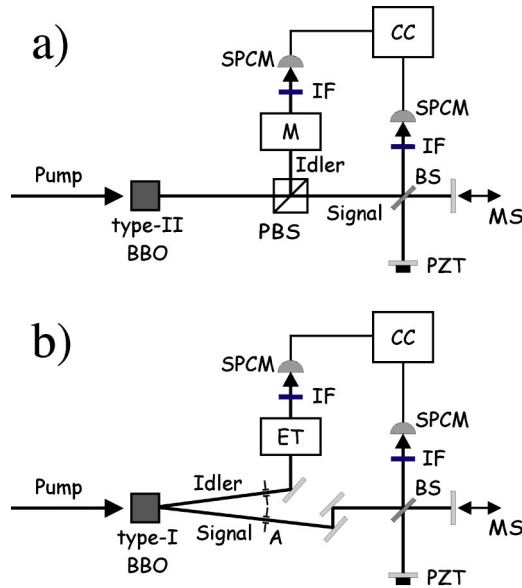


FIG. 1. Experimental setups: PBS, polarizing beam splitter; M, monochromator; A, aperture; ET, air-spaced etalons; BS, 50% beam splitter; MS, motorized translation stage; PZT, piezoelectric transducer; IF, interference filter; SPCM, single-photon counting module; and CC, coincidence counter.

plays a fundamental role in the measurements. We also demonstrate that by spectrally shaping the pump with the insertion of a further air-spaced etalon on its path without changing the filters in the idler channel, we can obtain a significantly different temporal shape for the signal autocorrelation function observed in coincidence. Finally, we present a complete theoretical model which describes, with a single equation, all the observed features, including the appearance of temporal and spectral fourth-order interference fringes and their exact behavior as a function of the different experimental parameters. Calculations taking into account the biphoton wave function generated in SPDC for type-I and type-II nonlinear crystals, the spectral pump shape with and without spectral filtering, and the different spectral or temporal filters on the idler and signal channels, show a very good agreement with experimental data.

II. EXPERIMENTAL SETUPS

We have performed three different sets of measurements using different crystals for SPDC and different systems for spectral filtering of both the idler and the pump beam. In the first case we use a type-II nonlinear crystal for SPDC and we spectrally filter the idler beam by means of a monochromator, while leaving the pump pulse unfiltered. Next, we use a type-I crystal and we filter the idler beam by means of air-spaced etalons. Finally, the latter setup is used in connection with a filtered pump pulse, obtained by placing a further etalon filter in the pump path.

Figure 1 shows a scheme of our experimental setups. The 1–5 ps long pulses from a mode-locked Ti:sapphire laser, operating around 788 nm at a repetition rate of 82 MHz, are frequency doubled in a LBO crystal to generate the pump

pulses at 394 nm for SPDC. In the setup of Fig. 1(a) the pump is mildly focused on a 3-mm-long BBO crystal cut for type-II collinear degenerate down-conversion. The two orthogonally polarized beams emerging from the crystal are recollimated and then separated by a polarizing beam splitter (for more details, see Ref. [21]). In the setup of Fig. 1(b) a 3-mm-long BBO crystal cut for type-I collinear degenerate down-conversion is pumped by a collimated beam. The crystal is slightly tilted from the collinear condition in order to get degenerate SPDC emission along a cone, and the signal and idler photons are then selected by two apertures (A).

In both setups, after spatial separation, one of the beams (that we will name “signal”) is directed to a stable Michelson interferometer with a piezoelectric transducer on one arm and a motorized translation stage on the other one, allowing us to finely control the relative path-length difference between the two optical paths. The other beam (the “idler”) is sent to a spectral filtering system: in setup (a) we use a 500-mm monochromator with a spectral resolution of 0.02 nm and a dispersion coefficient of 1.3 nm/mm; in setup (b) we use one or two air-spaced etalons (ET) with a finesse of 20 and coating wavelength of 786 nm, with cavity lengths of 25 μm and 100 μm . For some measurements we have also spectrally filtered the pump beam by placing a second air-spaced etalon with a cavity length of 250 μm , a finesse of 30, and a central wavelength of 393 nm, on the pump beam path.

At the exit of both the interferometer and the filtering system, the emerging beams are collected by means of 25 mm focal length GRIN (graded index) lenses, and detected by single-photon counting modules (SPCM, Perkin-Elmer AQR-12). Interference filters of various bandwidths (between 3 and 10 nm) are placed in front of the SPCMs in order to cut some of the background light. The signals from the two detectors can be either counted directly or in coincidence (within a 2 ns time window) as a function of the experimental parameters.

In both the experimental setups illustrated in Fig. 1 we performed conditioned measurements of the signal linear autocorrelation function by recording the coincidence counts as a function of the relative path-length difference between the two arms of the interferometer for different settings of the spectral filters: either different monochromator output slit widths or different etalons. With the apparatus depicted in Fig. 1(a), we could also perform conditioned measurements of the idler spectrum by scanning the monochromator central wavelength for different values of the relative path-length difference between the two interferometer arms.

III. THEORETICAL DESCRIPTION

A. Spontaneous parametric down-conversion with a pulsed pump

In the spontaneous parametric down-conversion process one pump photon with frequency ω_p impinging on a $\chi^{(2)}$ nonlinear crystal decays into two lower-frequency photons called signal and idler, provided that the energy and momentum conservation laws (or phase-matching conditions) are satisfied. The phase-matching conditions can be fulfilled in-

side the crystal in two different ways depending on how the two emitted photons are polarized. In type-I interaction the output photons are polarized in the same direction as ordinary waves. Alternatively, in type-II interaction, the signal and idler propagate inside the crystal as ordinary and extraordinary waves, respectively, and are orthogonally polarized with respect to each other.

In recent years, the SPDC process has been studied extensively when excited by a continuous [22–24] or a pulsed [25–31] pump. Here, we give a basic description of the SPDC process pumped by a picosecond pulsed laser source following the description given in Refs. [23,25,27]. We consider the case where the signal and idler are collinear with the pump in order to neglect the transverse components of the fields and give a one-dimensional description. Although this condition is not satisfied in several instances, the small-emission angles of the signal and idler beams in our experimental apparatus allow the collinear description of SPDC to well approximate our experimental results.

From the interaction Hamiltonian, the state emitted by the SPDC process is calculated to first order in perturbation theory as

$$|\Psi\rangle = |0\rangle + \alpha \int d\omega_s d\omega_i d\omega_p \delta(\omega_p - \omega_i - \omega_s) \mathcal{E}_p^{(+)}(\omega_p) \times \int_0^L dz e^{-i(k_p - k_i - k_s)z} |\omega_s\rangle_s |\omega_i\rangle_i \quad (1)$$

$$= |0\rangle + \int d\omega_s d\omega_i \psi(\omega_s, \omega_i) |\omega_s\rangle_s |\omega_i\rangle_i, \quad (2)$$

where the state vector $|\omega\rangle_j$ represents the single-photon state with frequency ω in the mode j and the function $\psi(\omega_s, \omega_i)$ is defined as

$$\psi(\omega_s, \omega_i) = \alpha \mathcal{E}_p^{(+)}(\omega_s + \omega_i) \frac{\sin(\Delta k L/2)}{\Delta k L/2} e^{-i\Delta k L/2}, \quad (3)$$

where L is the crystal length, Δk the phase-mismatch factor, and α includes the constants and the slowly varying terms. In the above expression the pump amplitude $\mathcal{E}_p^{(+)}(\omega)$ is considered to be a classical quantity propagating in the z direction, and the chirp-free pulsed pump is assumed to have a Gaussian profile:

$$\mathcal{E}_p^{(+)}(\omega) = \exp\left(-\frac{(\omega - \omega_p^0)^2}{4\sigma_p^2}\right), \quad (4)$$

with a FWHM $\Delta\omega_p = 2\sqrt{2 \ln 2} \sigma_p$ and a central frequency ω_p^0 .

The phase-mismatch factor $\Delta k = k_p(\omega_p) - k_i(\omega_i) - k_s(\omega_s)$ is approximated to the second-order term of the expansion around the phase-matching frequencies according to Refs. [25–29],

$$k_j(\omega_j) = k_j(\omega_j^0) + k_j'(\omega_j^0)(\omega_j - \omega_j^0) + \frac{1}{2}k_j''(\omega_j^0)(\omega_j - \omega_j^0)^2, \quad (5)$$

$j = p, s, i,$

where ω_j^0 ($j = p, s, i$) are the central frequencies for the pump,

signal, and idler fields, respectively, which we assume to obey the perfect phase-matching conditions, $k_p(\omega_p^0) - k_i(\omega_i^0) - k_s(\omega_s^0) = 0$ and $\omega_p^0 - \omega_i^0 - \omega_s^0 = 0$. The inverse of group velocity is $k_j'(\omega_j) = dk_j/d\omega_j$ and the group-velocity dispersion is introduced by the second-order coefficient $k_j''(\omega_j) = d^2k_j/d\omega_j^2$.

The phase mismatch can be approximated in different ways according to the type of nonlinear interaction inside the crystal. For a degenerate type-I situation, where the signal and idler photons have $k_i' = k_s'$ and $k_i'' = k_s''$, the phase mismatch is given by $|\Delta k| \approx k_s'' \Omega^2$, where $\omega_s = \omega_s^0 + \Omega$ and $\omega_i = \omega_i^0 - \Omega$. In a type-II interaction, the second-order terms of the expansion are negligible and we can thus approximate the phase mismatch to $|\Delta k| \approx (k_i' - k_s')\Omega$.

B. Spectral and temporal shaping of entangled photons

We consider the case where the signal and idler photons are spatially separated and the idler is directed to a spectral filter, while the signal travels through a Michelson interferometer with a variable delay between the two arms. At the outputs of both the spectral filter and the interferometer, a couple of single-photon counting modules is inserted, and their coincidence counts are measured.

When one idler photon is detected, the SPDC wave function (2) collapses onto a single-photon signal state whose characteristics depend on the kind of measurement performed on the idler. Detection of the filtered idler photon thus reduces the SPDC state into the single-photon state described by the partial trace of the product between the SPDC state density operator $\hat{\rho}$ and the measurement density operator $\hat{\rho}_i$,

$$\hat{\rho}_s = \text{Tr}_i(\hat{\rho}_i \hat{\rho}), \quad (6)$$

where $\hat{\rho} = |\Psi\rangle\langle\Psi|$ is the density operator for the pure SPDC state $|\Psi\rangle$ [32], and the single-photon detection of the filtered idler beam is described by the diagonal density operator [33]

$$\hat{\rho}_i = \int d\omega T(\omega - \omega_m) F_i(\omega) |\omega\rangle_i \langle\omega|_i. \quad (7)$$

The function $T(\omega - \omega_m)$ is the transmission of the spectral filter with center frequency ω_m , and $F_i(\omega)$ is the transmission function which describes the interference filter placed in front of the idler detector. Therefore, after the detection of the idler photon, the two-photon state collapses into the state described by

$$\hat{\rho}_s = \int d\omega_s d\omega_s' d\omega_i T(\omega_i - \omega_m) F_i(\omega_i) \times \psi^*(\omega_s', \omega_i) \psi(\omega_s, \omega_i) |\omega_s'\rangle_s \langle\omega_s|_s \quad (8)$$

and the signal-photon detection probability, conditioned on the detection of the filtered idler photon, is given by the correlation function

$$G(t) = \langle \hat{E}_s^{(-)}(t) \hat{E}_s^{(+)}(t) \rangle \quad (9)$$

$$= \text{Tr}[\hat{\rho}_s \hat{\rho}_{F_s} \hat{E}_s^{(-)}(t) \hat{E}_s^{(+)}(t)], \quad (10)$$

where $\hat{E}_s^{(+)}(t)$ is the electric-field operator after the Michelson interferometer, which is written as a function of the unbalancing time τ of the interferometer as

$$\hat{E}_s^{(+)}(t) = \mathcal{RT} \int d\omega \hat{a}_s(\omega) (1 + e^{i\omega\tau}) e^{i\omega t}, \quad (11)$$

where $\hat{a}_s(\omega)$ is the field annihilation operator and \mathcal{R} and \mathcal{T} are the complex reflectivity and transmittivity coefficients of the beam splitter, respectively. The operator $\hat{\rho}_{F_s}$ describes the action of the interference filter placed in front of the signal detector and is written as

$$\hat{\rho}_{F_s} = \int d\omega F_s(\omega) |\omega\rangle_s \langle \omega|_s. \quad (12)$$

The coincidence rate is proportional to the integral of the correlation function $G(t)$ with respect to t over the electronic coincidence window of width T_c [34]. Generally, the coincidence window is much larger than the coherence time of the emitted photons, therefore, by letting $T_c \rightarrow \infty$, the coincidence rate results proportional to

$$\begin{aligned} R_c(\tau, \omega_m) &= \int_{-\infty}^{\infty} dt G(t) \quad (13) \\ &= 2|\mathcal{RT}|^2 \int d\omega_s d\omega_i |\psi(\omega_s, \omega_i)|^2 F_i(\omega_i) F_s(\omega_s) \\ &\quad \times T(\omega_i - \omega_m) (1 + \cos \omega_s \tau). \quad (14) \end{aligned}$$

This equation expresses the convolution of the SPDC emission probability $|\psi(\omega_s, \omega_i)|^2$ with the transmission function of the filters and the spectral response of the Michelson interferometer. When the filter central frequency ω_m is fixed and one arm of the interferometer is scanned, one can observe the correlation function of the filtered two-photon state, which comes from the spectral convolution of the SPDC wave function with the filter transmission function $T(\omega - \omega_m)$. On the other hand, if the interferometer is kept unbalanced ($\tau \neq 0$) and the central frequency of the filter ω_m is scanned, then idler spectral fringes are observed with a period inversely proportional to τ .

These fourth-order interference effects are often referred to as ghost interferences, since they only appear when the coincidence counts from the signal and idler detectors are observed. In particular, the case described above is the energy-time analogous of the ghost interferences observed in the spatial domain by Refs. [14,15]; here the single spatial slit is replaced by the spectral window of the monochromator, while the unbalanced Michelson interferometer plays the role of a temporal Young's double slit.

For monochromatic pump radiation, SPDC generates perfect frequency entangled states: in such a case the coherence time of the filtered two-photon state can be extended to infinity, provided that a monochromatic filtering is performed on the idler photon. In exactly the same way, one can in

principle obtain narrower and narrower fourth-order spectral interference fringes by using infinitely long unbalancing delays on the Michelson interferometer. However, if the coherence time of the pump is finite, then it becomes the limiting factor and, according to Eq. (14), the coherence time of the filtered two-photon state (or conditioned signal state) cannot exceed its value. To put it in simple terms, one cannot increase the precision in the measurement of the signal frequency by a better knowledge of the idler frequency because the bandwidth of the pump is, in any case, the lower limit for the achievable resolution of the signal spectrum. Accordingly, the visibility of the spectral fringes is degraded when the interferometer unbalancing time τ is made longer than the pump coherence time, i.e., when the spacing of the spectral fringes becomes smaller than the pump bandwidth.

Different kinds of spectral filters have been used for our measurements. In one case we have inserted a monochromator filter with variable width and variable central frequency as described in Ref. [21]. The monochromator transmission function is the convolution product of two rectangular functions corresponding to the input and output apertures of the monochromator. The result is a trapezoid with the major base equal to the sum of the two rectangular widths and with the minor base equal to the difference between the two rectangular widths. Alternatively, we have used etalon filters, which provide a different and peculiar nonlocal spectral-temporal shaping. These filters are characterized by a large number of very narrow transmission lines, with an overall transmission function given by

$$T(\omega) = \left\{ 1 + \frac{4\mathcal{F}^2}{\pi^2} \sin^2 \left[\frac{\pi\omega}{\Omega} \right] \right\}^{-1}, \quad (15)$$

where $\Omega/2\pi$ and \mathcal{F} are the FSR and the finesse of the resonator, respectively. The presence of one or more etalon transmission peaks under the transmission curve of the interference filters drastically changes the induced spectral-temporal shape of the signal photon.

In order to study the effects of the pump coherence time, we manipulated it by placing a further etalon filter on the pump beam path. The resulting pump spectrum is simply obtained by multiplying the original pump spectral profile by the transmission function of the etalon. The action of the pump filter extends the coherence time of the two-photon state as shown by Eq. (14). Moreover, as it will be shown later in this paper, when more than one transmission peaks of the pump etalon come into play, additional beating effects appear in the fourth-order interference envelope.

Finally, the interference filters placed in front of the detectors in order to limit background light are assumed to have a Gaussian shape:

$$F_j(\omega) = \exp\left(-\frac{(\omega - \omega_{F_j}^0)^2}{2\sigma_{F_j}^2}\right), \quad j = i, s, \quad (16)$$

with a FWHM $\Delta\omega_{F_j} = 2\sqrt{2 \ln 2} \sigma_{F_j}$ and a central frequency $\omega_{F_j}^0$.

IV. RESULTS AND DISCUSSION

A. Monochromator filter

For the first set of measurements, we have used the setup shown in Fig. 1(a), with a 3-mm-type-II BBO nonlinear crystal and a monochromator in the idler-beam path as the spectral filter. We have performed coincidence measurements of the signal autocorrelation function for different values of the monochromator spectral resolution and coincidence measurements of the idler spectrum for different delays between the arms of the interferometer in the signal path.

We have shown [21] that when observations are made in coincidence the selection of a narrow spectrum for the idler photons leads to a broadening of the signal autocorrelation function and fourth-order temporal interference fringes are detected also for delays much longer than the signal coherence time. Alternatively, we have shown that fourth-order interference fringes appear in the idler spectrum conditioned on the detection of the signal photon after the unbalanced Michelson interferometer.

Both the coincidence measurements of signal autocorrelation function and idler spectrum can be calculated from Eq. (14). In this case $T(\omega)$ is the monochromator transmission function: a trapezoidal function (which reduces to a triangular shape when the input and output slits have the same width) with a FWHM given by the product between the monochromator dispersion of 1.3 nm/mm and the larger slit width. $F_i(\omega)$ and $F_s(\omega)$ are the transmission functions of the two interference filters placed in front of the SPCMs, given in Eq. (16) with central wavelengths $\lambda_{Fi}^0 = 785.4$ nm and $\lambda_{Fs}^0 = 786.0$ nm, and widths $\Delta\lambda_{Fi} = 5.4$ nm (FWHM) and $\Delta\lambda_{Fs} = 5.5$ nm (FWHM). The function $\psi(\omega_s, \omega_i)$ can be calculated considering that the pulsed pump spectral amplitude $\mathcal{E}_p^{(+)}$ is given by Eq. (4) with central wavelength $\lambda_p^0 = 394$ nm and FWHM $\Delta\lambda_p = 0.078$ nm; Δk is calculated for type-II interaction with $|k'_s - k'_i| = 0.06/c$. Finally, L can be replaced by the effective interaction length $L_{\text{eff}} = 1.3$ mm, which is calculated by taking into account the walk-off angle of the BBO crystal and the pump beam waist.

Figure 2 shows the visibility of fourth-order temporal interference fringes recorded for four different settings of the monochromator slits. The experimental fringe visibility is measured by changing the delay between the two arms of the interferometer in coarse steps; for each position, a fine-scan acquisition of 40 points is performed while moving one arm of the interferometer by means of a piezoelectric transducer driven by a ramp function generator. The solid lines in Fig. 2 show the theoretical visibility curves calculated from the autocorrelation function obtained from Eq. (14), while keeping $\lambda_m = 2\pi c / \omega_m = 788$ nm as fixed and scanning the unbalancing time τ for the different filter widths. Note that increasing the spectral filtering of the idler photon from 1.3 nm to 0.13 nm [from case (a) to case (c) of Fig. 2] the signal coherence time rapidly increases from 0.9 ps to 2.6 ps. A further narrowing of the idler filter [from case (c) to (d) of Fig. 2] does not produce a corresponding increase of the coherence time, due to the fact that, when the width of the monochromator spectral filter is reduced below the pump bandwidth, it is the coherence time of the pump pulses (about 2.9 ps in this case)

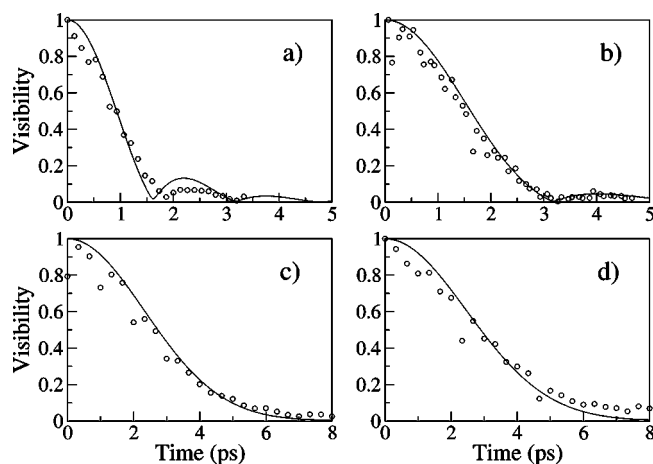


FIG. 2. Experimental visibility (circles) of the fourth-order temporal interference fringes on the signal beam for different widths of the monochromator slit on the idler channel: (a) output width of 1000 μm and input width of 100 μm (the transmission function is a trapezoid with FWHM of 1.3 nm); (b) output width of 500 μm and input width of 100 μm (the transmission function is a trapezoid with FWHM of 0.65 nm); (c) output width of 100 μm and input width of 100 μm (the transmission function is a triangle with FWHM of 0.13 nm); (d) output width of 50 μm and input width of 50 μm (the transmission function is again a triangle with FWHM of 0.065 nm). The solid curves are the theoretical visibilities calculated according to Eq. (14).

which is the limiting factor for the signal coherence time. The broadening of the signal autocorrelation function for different values of the frequency filter is well described by the theoretical calculations based on Eq. (14), where the dependence on the spectral width of the pump (σ_p) is contained in the $\psi(\omega_s, \omega_i)$ term.

Spectral interference fringes on the idler spectrum conditioned by the detection of a signal photon after the Michelson interferometer are shown in Fig. 3, for different time delays between the interferometer arms.

Figures 3(a) and 3(c) show the experimental data obtained while scanning the monochromator central frequency for a fixed delay between the interferometer arms. Figures 3(b) and 3(d) show the corresponding theoretical curves derived from Eq. (14), calculated by keeping the delay τ fixed at the experimental values and varying ω_m . The good agreement between the experimental data and the theoretical curves is a demonstration of the correctness and completeness of our model description.

B. Etalon filters

For the second set of measurements we have used the setup of Fig. 1(b) with a 3-mm-type-I BBO nonlinear crystal. Air-spaced etalons are now used as the frequency filters instead of the monochromator. In this case we have measured the signal autocorrelation function conditioned by the detection of an idler photon after various filter combinations. Again, the conditioned signal autocorrelation function can be calculated from Eq. (14). The interference filters placed in front of the SPCMs still have Gaussian transmission func-

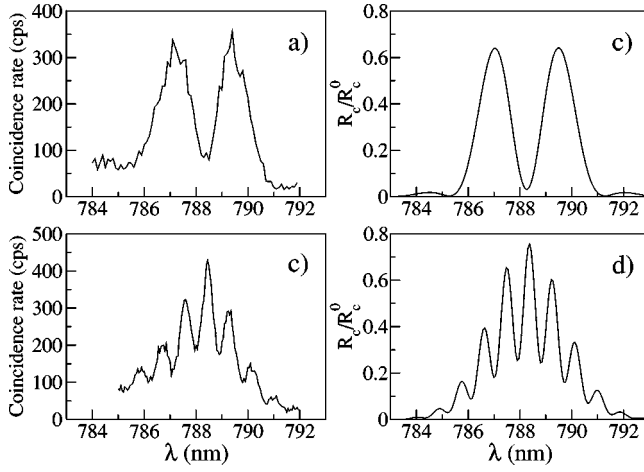


FIG. 3. Fourth-order spectral interference fringes on the idler spectrum for different time delays between the arms of the interferometer placed on the signal path: 700 fs in both pictures (a) (experimental data) and (b) (theoretical calculation), and 2300 fs in both pictures (c) (experimental data) and (d) (theoretical calculation). Experimental data [(a) and (c)] are taken with monochromator slit widths of 100 μm (input) and 250 μm (output). Theoretical curves [(b) and (d)] are calculated according to Eq. (14) and are normalized to $R_c^0 = R_c(0, \omega_i^0)$.

tions $F_i(\omega)$ and $F_s(\omega)$ [see Eq. (16)], but with slightly different widths and central frequencies: $\lambda_{Fi}^0 = 784.0$ nm and $\Delta\lambda_{Fi} = 9.8$ nm (for the filter on the idler path); $\lambda_{Fs}^0 = 785.0$ nm and $\Delta\lambda_{Fs} = 4.1$ nm (for the filter on the signal path). The filtering function $T(\omega)$ is now given by the etalon transmission function of Eq. (15). In particular, we have used two different etalon filters, ET1 (with FSR $\Lambda_1 = 12$ nm and FWHM $\Delta\lambda_1 = 0.6$ nm) and ET2 (with FSR $\Lambda_2 = 3$ nm and FWHM $\Delta\lambda_2 = 0.15$ nm), both for a wavelength of 786 nm and with a finesse $\mathcal{F} = 20$.

For the calculation of the function $\psi(\omega_s, \omega_i)$ we now consider a pump pulse with $\lambda_p^0 = 393$ nm and $\Delta\lambda_p = 0.25$ nm; Δk is obtained for the case of type-I interaction with $k_s'' = 7.7 \times 10^{-26}$ s²/m and $L = 3$ mm. Note that the pump bandwidth in this case is larger than in the first series of experiments because we now use significantly shorter pulses from the mode-locked laser.

When the etalon filter ET1 is placed in the idler path, we do not observe substantial differences with respect to the case when filtering was performed by the monochromator. In this case the FSR of the etalon resonator is larger than the width of the interference filter placed on the idler channel ($\Lambda_1 > \Delta\lambda_{Fi}$), so that their combined action only allows transmission through a single narrow wavelength interval of width $\Delta\lambda_1$, similar to the monochromator case. The coincidence signal coherence time is found to be 0.69 ± 0.2 ps, which is significantly smaller than the one recorded with the monochromator at similar FWHM because of the larger pump spectral width in this second series of measurements.

If the ET2 filter is used, the signal autocorrelation function still shows the expected additional broadening (from 0.69 to 0.82 ± 0.2 ps) due to the spectral narrowing by the etalon transmission peaks but, besides it, one also observes the appearance of further modulations in the temporal profile

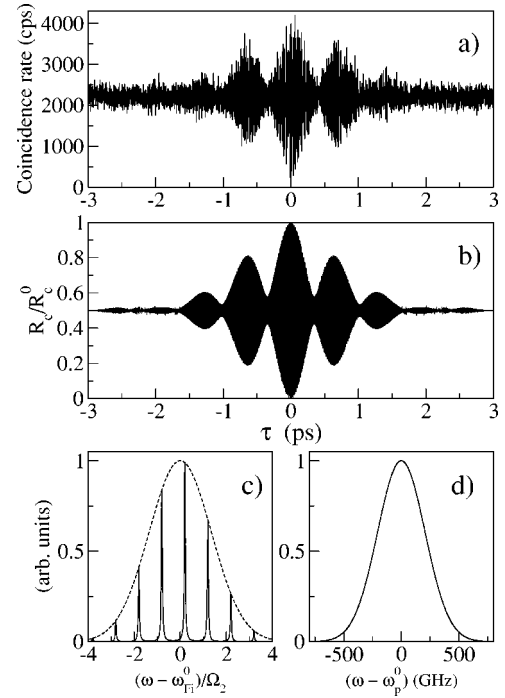


FIG. 4. Signal correlation function conditioned on the detection of an idler photon after the etalon filter ET2 (see text): (a) experimental data; (b) theoretical simulation according to Eq. (14) normalized to $R_c^0 = R_c(0, \omega_i^0)$; (c) calculated transmission function of the idler interference filter and etalon combination (the dashed curve is the transmission curve for the interference filter alone); (d) calculated pump spectrum as used in the simulations: the pump is not spectrally filtered in this case.

of the fringe contrast. The situation with the etalon filter ET2 is indeed quite different: in this case, the FSR of the resonator is smaller than the bandwidth of the interference filter in front of the idler detector ($\Lambda_2 < \Delta\lambda_{Fi}$), and more transmission peaks contribute to the detected idler spectrum [see Fig. 4(c)]. In this case, the detection of an idler photon after ET2 collapses the SPDC two-photon state onto a state with a similarly modulated spectrum and periodic modulations in the temporal profile of its autocorrelation function are clearly to be expected. Of course, the shape and visibility of these temporal modulations depend on the mutual position between the etalon transmission peaks and the central frequency of the interference filter, and can be manipulated by tilting the resonator around an axis perpendicular to the beam propagation direction.

Note that if both ET1 and ET2 are placed together (and are properly tilted) on the idler beam path, then the filtered idler spectrum is at most composed of a single peak, as in the case of ET1, but with a width essentially given by $\Delta\lambda_2$. The temporal modulations in the signal autocorrelation thus vanish, whereas its coherence time does not change dramatically (from 0.82 to 0.86 ± 0.2 ps), being again essentially determined by the temporal coherence of the pump (see Fig. 6).

One can also look at the effect of the etalon filters from the temporal point of view. When the etalon FSR is larger than the pulse spectral width, then the temporal coherence of the pulse is longer than the round-trip time in the resonator,

and the tail of the pulse entering the cavity interferes with the leading edge of the pulse itself being doubly reflected inside. The net effect after the cavity is that of a temporal stretching of the pulse, which now contains only the frequencies that interfere constructively in the process. The detection of such a time-elongated idler pulse collapses the signal photon onto a similarly stretched state, which manifests itself in the stretching of the coincidence autocorrelation function. Conversely, when the FSR of the etalon is smaller than the pulse spectral width, then the idler coherence time is shorter than the round-trip time, and no temporal overlap is possible between the incoming pulse and its leading edge being reflected inside the resonator. At the exit of the etalon, a pulse train of decreasing amplitude appears, with an interpulse delay given by the cavity round trip. The detection of an idler photon then projects the signal state into a similarly time-modulated state which is made evident by the appearance of modulations in the coincidence autocorrelation curve.

In other words, in the latter case where $\Lambda_2 < \Delta\lambda_{Fi}$, one cannot know, not even in principle, if a recorded coincidence is due to a signal photon passing through the long interferometer arm with an idler photon making one or more round trips inside the cavity, or if it is due to a signal photon passing through the short interferometer arm with an idler photon directly transmitted by the cavity without internal reflections. These intrinsically indistinguishable paths to the same coincidence event produce interferences which appear as a modulation in the two-photon correlation function.

Figure 4(a) shows the measured signal correlation function obtained in coincidence, by filtering the idler photon with ET2 only. The modulation period corresponds to one round trip in the cavity of ET2 ($2\pi/\Omega_2=0.67$ ps) and the coherence time, defined as the half width at half maximum of the curve envelope, depends on both the pump spectral width $\Delta\lambda_p$ and the width of the ET2 transmission peaks $\Delta\lambda_2$. The narrowing of the etalon peak width from 0.6 to 0.15 nm yields an increase in the coherence time from 0.69 to 0.82 ps compared to the case with ET1 (see Fig. 6).

The theoretical signal correlation function can be obtained from Eq. (14) by varying the interferometer unbalancing time τ for different values of the offset frequency δ between the etalon central peak and the central frequency ω_{Fi}^0 of the interference filter. The position of the central transmission peak of the etalon is then defined as $\omega_m = \omega_{Fi}^0 + 2\pi\delta$. By comparing the experimental curve with the theoretical calculations, a good agreement is found when the etalon central peak is offset by about 300 GHz from ω_{Fi}^0 [see Fig. 4(c)]. Figure 4(b) shows this calculated signal correlation function with $\delta=300$ GHz.

C. Etalon filter on the pump

From Eq. (14) and from our previous discussion it is evident that the conditioned signal coherence time is determined not only by the spectral filtering on the idler channel, but also by the pump spectral shape. To verify this prediction we have filtered the pump with a UV etalon having a FSR $\Lambda_{UV}=0.3$ nm and FWHM $\Delta\lambda_{UV}=0.01$ nm at 393 nm [see Fig. 5(d)]. Figure 5(a) shows the experimental signal corre-

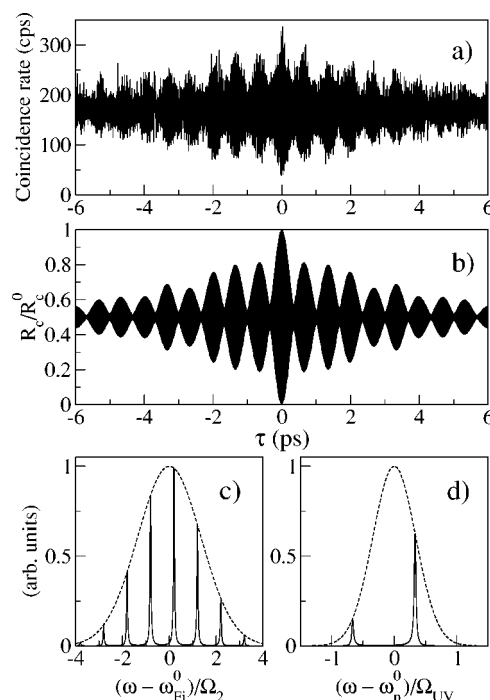


FIG. 5. Signal correlation function conditioned on the detection of an idler photon after the etalon filter ET2 with a spectrally filtered pump: (a) experimental data; (b) theoretical simulation according to Eq. (14) normalized to $R_c^0 = R_c(0, \omega_i^0)$; (c) calculated transmission function of the idler interference filter and etalon combination (the dashed curve is the transmission curve for the interference filter alone); (d) pump spectral profile after filtering by the UV etalon (the dashed curve is the unfiltered pump spectrum).

lation function obtained in coincidence, while filtering the idler photon by means of ET2 [Fig. 5(c)] and the pump by means of the UV etalon. Comparing Fig. 4(a) with Fig. 5(a), it is clear that decreasing the spectral width of the pump from 0.25 nm to 0.01 nm (corresponding to an increase of the pump coherence time from 0.92 to 11.4 ps) yields a broadening in the envelope of the conditioned signal correlation function, corresponding to an increase of the coherence time from about 0.82 to 3 ± 1 ps.

In Fig. 6 we present the measured and calculated coherence times of the two-photon state (or the conditioned coherence time of the signal photon) as a function of the spectral FWHM of the idler etalon filter. Three curves are plotted: the first corresponds to the unfiltered pump, the second to the pump filtered by the UV etalon, and the third to the ideal case of a monochromatic pump. The lower horizontal line gives the asymptotic behavior for very large etalon widths (without etalon on the idler, essentially), where the upper limit for the idler bandwidth is mainly determined by the width of the idler interference filter. On the contrary, the two upper horizontal lines represent the asymptotic behavior of the coherence times for small etalon widths, and correspond to the coherence times of the pump in the filtered and unfiltered cases. It is evident that by using a pump with a narrower spectrum the conditioned coherence time of the signal photon may get significantly longer. If a monochromatic pump were used in the experiments, the coherence time

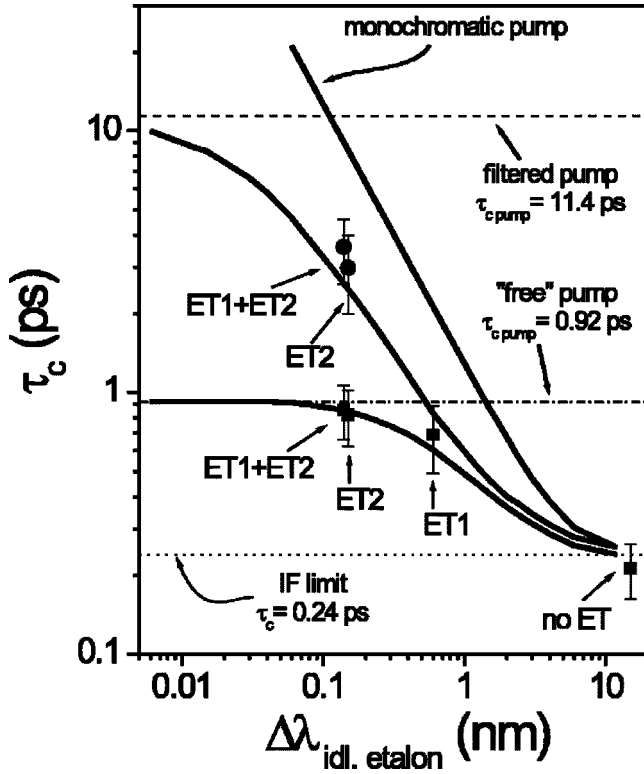


FIG. 6. Measured and calculated conditioned coherence time of the signal photon as a function of the idler etalon width for different spectral widths of the pump pulses. Square experimental points and lower theoretical curve, no filtering on the (“free”) pump; circle experimental points and middle theoretical curve, pump filtered by the UV etalon; upper theoretical curve, monochromatic pump. The upper horizontal line corresponds to the UV-etalon-filtered pump coherence time, while the middle one to the coherence time of the unfiltered pump. The lower horizontal line indicates the conditioned signal coherence time due to the interference filters only.

would have followed the upper curve, yielding an exact relationship (at least for narrow idler filtering) of inverse proportionality between the bandwidth of the idler spectral filter and the conditioned signal coherence time.

Figure 5(b) shows the theoretical signal correlation function calculated for the same parameters of Fig. 4(b), except for the pump spectral amplitude $\mathcal{E}_p^{(+)}(\omega)$, where the Gaussian shape is now replaced by the product between the Gaussian of Eq. (4) and the etalon transmission function $T(\omega - \omega_m)$ [given by Eq. (15)] with $\omega_m = \omega_p^0 + 2\pi\delta_{UV}$, where δ_{UV} indicates the mutual spectral position between the UV-etalon peak frequency and the central frequency ω_p^0 of the pump profile. A good agreement between the experimental data and the theoretical calculation is obtained for $\delta_{UV} = 200$ GHz [Fig. 5(b)].

It should be noted that both the theoretical and the experimental shapes show a slight modulation, with a very low visibility, superposed to the modulation due to ET2, and with a longer period. This further large-scale modulation is connected with the pump etalon, and its period is indeed the inverse of the FSR of the UV etalon ($2\pi/\Omega_{UV} = 1.7$ ps). The low visibility is associated to δ_{UV} : For $\delta_{UV} = 200$ GHz, one transmission peak of the etalon is not far from the center of

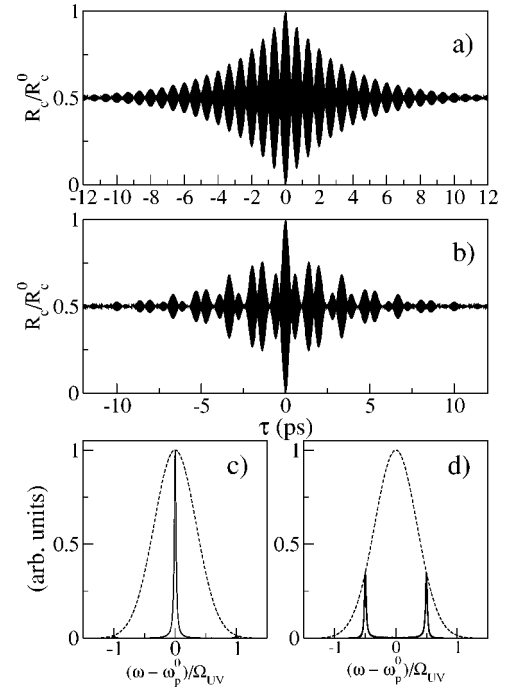


FIG. 7. Theoretical signal conditioned autocorrelation calculated according to Eq. (14), normalized to $R_c^0 = R_c(0, \omega_t^0)$, in the conditions where the idler photon is spectrally filtered with etalon ET2 and the pump is spectrally filtered with an UV etalon (see text). The curves are calculated for different values of the mutual spectral position (δ_{UV}) between the UV-etalon peak frequency and the central frequency of the pump profile: (a) $\delta_{UV} = 0$ GHz, (b) $\delta_{UV} = 300$ GHz. The corresponding filtered pump spectra are shown in (c) and (d).

the pump spectrum, while a second one only transmits a tail of the pump spectral distribution [see Fig. 5(d)]. In order to verify this assumption we have calculated the signal correlation function in the same conditions of Fig. 5(b), but changing δ_{UV} in order to have just one or two symmetric etalon peaks under the Gaussian pump envelope.

In Fig. 7 we show the theoretical signal autocorrelation calculated when both the idler beam and the pump beam are spectrally filtered, respectively with ET2 and with the UV etalon for $\delta_{UV} = 0$ GHz [Fig. 7(a)] and $\delta_{UV} = 300$ GHz [Fig. 7(b)]. In the condition $\delta_{UV} = 0$ GHz, where the central etalon peak is coincident with the center of the pump spectral profile [see Fig. 7(c)], the filtered pump spectrum is essentially composed of a single peak and no other modulation appears apart from those connected with the idler etalon ET2; differently, for $\delta_{UV} = 300$ GHz two-symmetric etalon peaks are present under the pump profile [see Fig. 7(d)] and the visibility of the large-scale modulation is much more evident.

V. CONCLUSIONS

We have performed a systematic experimental and theoretical investigation of the energy-time entanglement properties of a two-photon state generated by spontaneous parametric down-conversion. By using different configurations for the generation of the entangled pair and for the spectral or

temporal shaping of one of the two photons, we have observed the nonlocal changes in the autocorrelation or in the spectrum of the other by coincidence measurements. Either a monochromator (as in our previous experiments [21]) or etalon filters with different characteristics have been used to spectrally and temporally shape the idler photon while observing the conditioned signal autocorrelation by a Michelson interferometer. Conversely, the unbalanced interferometer has been used to shape the signal photon while measuring the conditioned idler spectrum by the monochromator. The use of a pulsed laser source has allowed us to bring to evidence the effects of a finite pump bandwidth in the process; to further investigate them, the pump spectrum has been manipulated by means of etalon filters, and we have observed the corresponding modulations in the two-photon correlation function. An accurate theoretical description of the underlying processes has been presented and we have

been able to completely and precisely reproduce all our measured data, regardless of the variety of experimental configurations adopted.

These results will be of interest for an accurate engineering of quantum states and for the realization of more elaborated nonlocal shaping techniques, which may prove useful both for fundamental tests of quantum mechanics and for the development of new experimental schemes for applications.

ACKNOWLEDGMENTS

This work was supported by the Italian Ministry of University and Scientific Research (MIUR). The authors would also like to thank the Department of Physics of the University of Florence for the kind hospitality and F. Marin for useful discussions.

-
- [1] A. Einstein, B. Podolsky, and N. Rosen, *Phys. Rev.* **47**, 777 (1935).
- [2] J. S. Bell, *Physics* (Long Island City, N.Y.) **1**, 195 (1964).
- [3] D. C. Burnham and D. L. Weinberg, *Phys. Rev. Lett.* **25**, 1970 (1970).
- [4] A. Aspect, J. Dalibard, and G. Roger, *Phys. Rev. Lett.* **49**, 1804 (1982).
- [5] Y. H. Shih and C. O. Alley, *Phys. Rev. Lett.* **61**, 2921 (1988).
- [6] Z. Y. Ou and L. Mandel, *Phys. Rev. Lett.* **61**, 50 (1988).
- [7] T. E. Kiess, Y. H. Shih, A. V. Sergienko, and C. O. Alley, *Phys. Rev. Lett.* **71**, 3893 (1993).
- [8] J. D. Franson, *Phys. Rev. Lett.* **62**, 2205 (1989).
- [9] Z. Y. Ou, X. Y. Zou, L. J. Wang, and L. Mandel, *Phys. Rev. Lett.* **65**, 321 (1990).
- [10] P. G. Kwiat, W. A. Vareka, C. K. Hong, H. Nathel, and R. Y. Chiao, *Phys. Rev. A* **41**, 2910 (1990).
- [11] J. Brendel, E. Mohler, and W. Martienssen, *Phys. Rev. Lett.* **66**, 1142 (1991).
- [12] J. G. Rarity and P. R. Tapster, *Phys. Rev. A* **45**, 2052 (1992).
- [13] P. G. Kwiat, A. M. Steinberg, and R. Y. Chiao, *Phys. Rev. A* **47**, R2472 (1993).
- [14] D. V. Strekalov, A. V. Sergienko, D. N. Klyshko, and Y. H. Shih, *Phys. Rev. Lett.* **74**, 3600 (1995).
- [15] R. Christanell, H. Weinfurter, and A. Zeilinger, *The Technical Digest of the European Quantum Electronic Conference EQEC's 93, Florence, 1993* (unpublished), p. 827.
- [16] P. H. Souto Ribeiro and G. A. Barbosa, *Phys. Rev. A* **54**, 3489 (1996).
- [17] E. J. S. Fonseca, P. H. Souto Ribeiro, S. Padua, and C. H. Monken, *Phys. Rev. A* **60**, 1530 (1999).
- [18] D. N. Klyshko, *Phys. Lett. A* **128**, 133 (1988).
- [19] L. M. Davis, *Phys. Lett. A* **140**, 275 (1989).
- [20] X. Y. Zou, T. P. Grayson, and L. Mandel, *Phys. Rev. Lett.* **69**, 3041 (1992).
- [21] M. Bellini, F. Marin, S. Viciani, A. Zavatta, and F. T. Arecchi, *Phys. Rev. Lett.* **90**, 043602 (2003).
- [22] C. K. Hong and L. Mandel, *Phys. Rev. A* **31**, 2409 (1985).
- [23] M. H. Rubin, D. N. Klyshko, Y. H. Shih, and A. V. Sergienko, *Phys. Rev. A* **50**, 5122 (1994).
- [24] M. H. Rubin, *Phys. Rev. A* **54**, 5349 (1996).
- [25] T. E. Keller and M. H. Rubin, *Phys. Rev. A* **56**, 1534 (1997).
- [26] Z. Y. Ou, *Quantum Semiclassic. Opt.* **9**, 599 (1997).
- [27] W. P. Grice and I. A. Walmsley, *Phys. Rev. A* **56**, 1627 (1997).
- [28] J. Peřina, Jr., A. V. Sergienko, B. M. Jost, B. E. A. Saleh, and M. C. Teich, *Phys. Rev. A* **59**, 2359 (1999).
- [29] R. Erdmann, D. Branning, W. Grice, and I. A. Walmsley, *Phys. Rev. A* **62**, 053810 (2000).
- [30] Y.-H. Kim, M. V. Chekhova, S. P. Kulik, M. H. Rubin, and Y. Shih, *Phys. Rev. A* **63**, 062301 (2001).
- [31] Y. Nambu, K. Usami, Y. Tsuda, K. Matsumoto, and K. Nakamura, *Phys. Rev. A* **66**, 033816 (2002).
- [32] D. V. Strekalov, Y.-H. Kim, and Y. Shih, *Phys. Rev. A* **60**, 2685 (1999).
- [33] T. Aichele, A. I. Lvovsky, and S. Schiller, *Eur. Phys. J. D* **18**, 237 (2002).
- [34] L. Mandel and E. Wolf, *Optical Coherence and Quantum Optics* (Cambridge University Press, Cambridge, England, 1995).